Supplementary Information (SI) for Journal of Materials Chemistry A.

Reducing the hydrogen transfer barrier by introduction of Ru *via* constructed Ir-Ru-$WO_{2.72}$ bridge for highly CO-tolerant hydrogen oxidation

Xu Yu[1,2,#], Han Tian[1,#], Ziyi Yu[1], Fantao Kong[1], Chang Chen[1,2], Ziwei Chang[4], Jian Huang[1], Xiangzhi Cui[1,2,3] *, Jianlin Shi[1,2]

[1] Shanghai Institute of Ceramics, Chinese Academy of Sciences, Shanghai 200050, PR China

[2] Center of Materials Science and Optoelectronics Engineering, University of Chinese Academy of Sciences, Beijing 100049, PR China

[3] School of Chemistry and Materials Science, Hangzhou Institute for Advanced Study, University of Chinese Academy of Sciences, Hangzhou 310024, PR China

[4] School of Physical Science and Technology, Shanghai Tech University, Shanghai 201210, PR China

*Email: cuixz@mail.sic.ac.cn

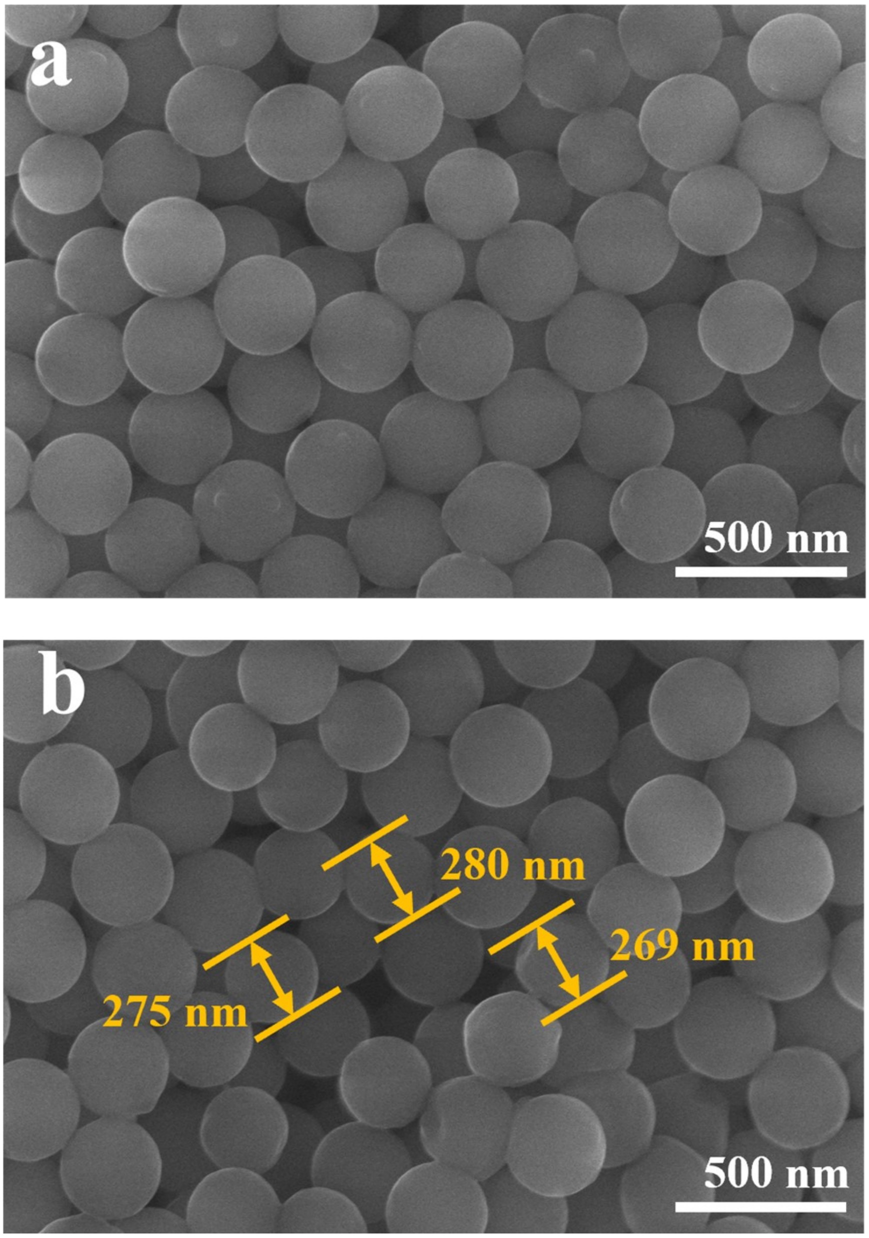

Figure S1. (a-b) SEM images of PS template.

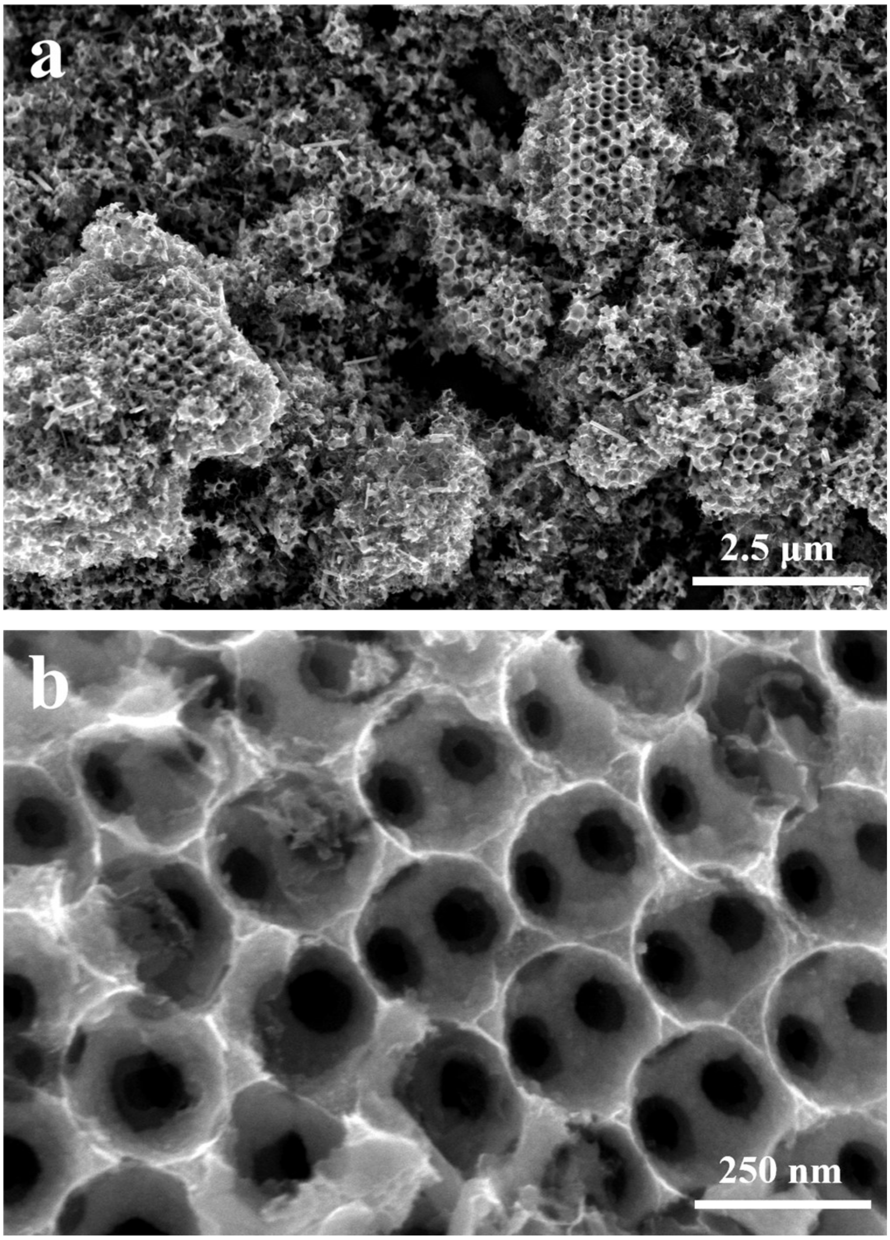

Figure S2. (a-b) SEM images of $WO_{2.72}$-C at different magnifications.

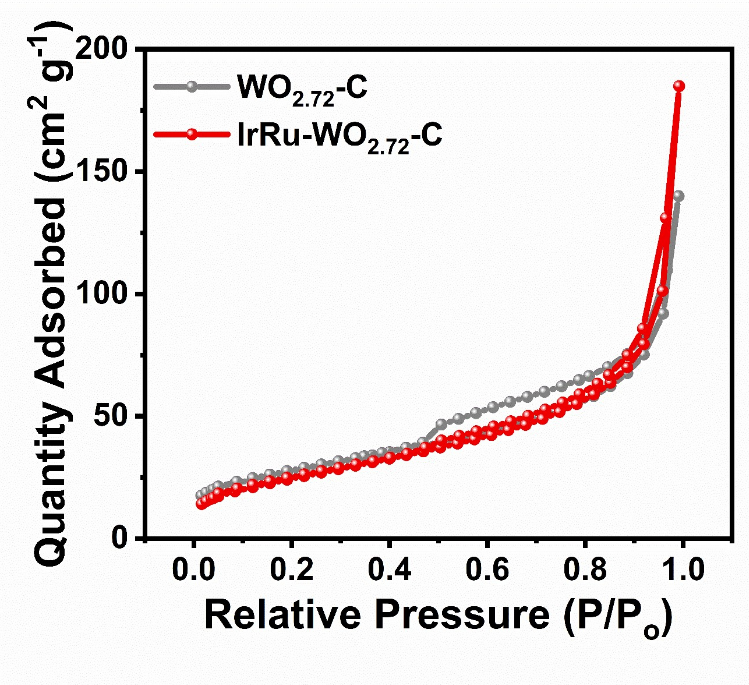

Figure S3. N_2 adsorption-desorption isotherms of $WO_{2.72}$-C and IrRu-$WO_{2.72}$-C.

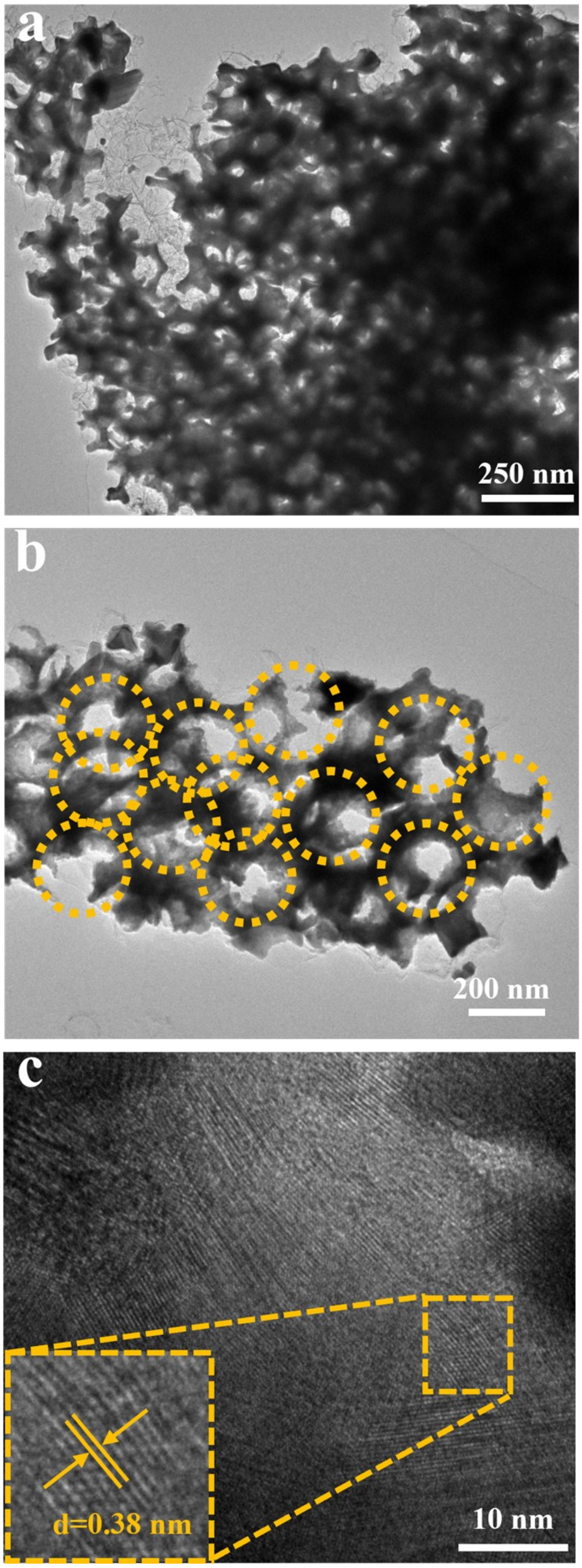

Figure S4. (a-b) TEM images of $WO_{2.72}$-C at different magnifications and the corresponding (c) HRTEM images. The d≈0.38 nm is assigned to the (010) plane of monoclinic $WO_{2.72}$.

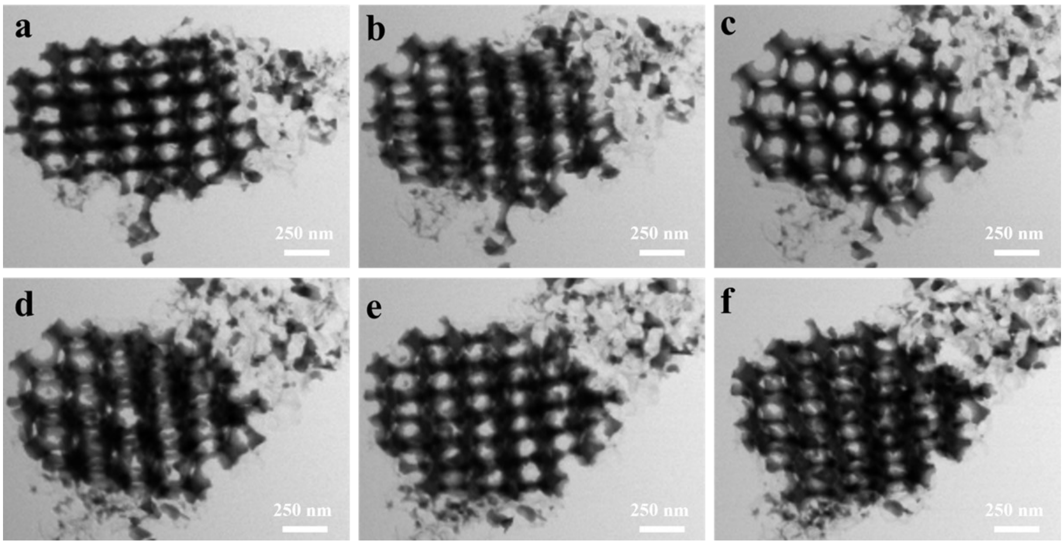

Figure S5. (a-d) Bright field (BF) STEM images of $WO_{2.72}$-C at different angles,

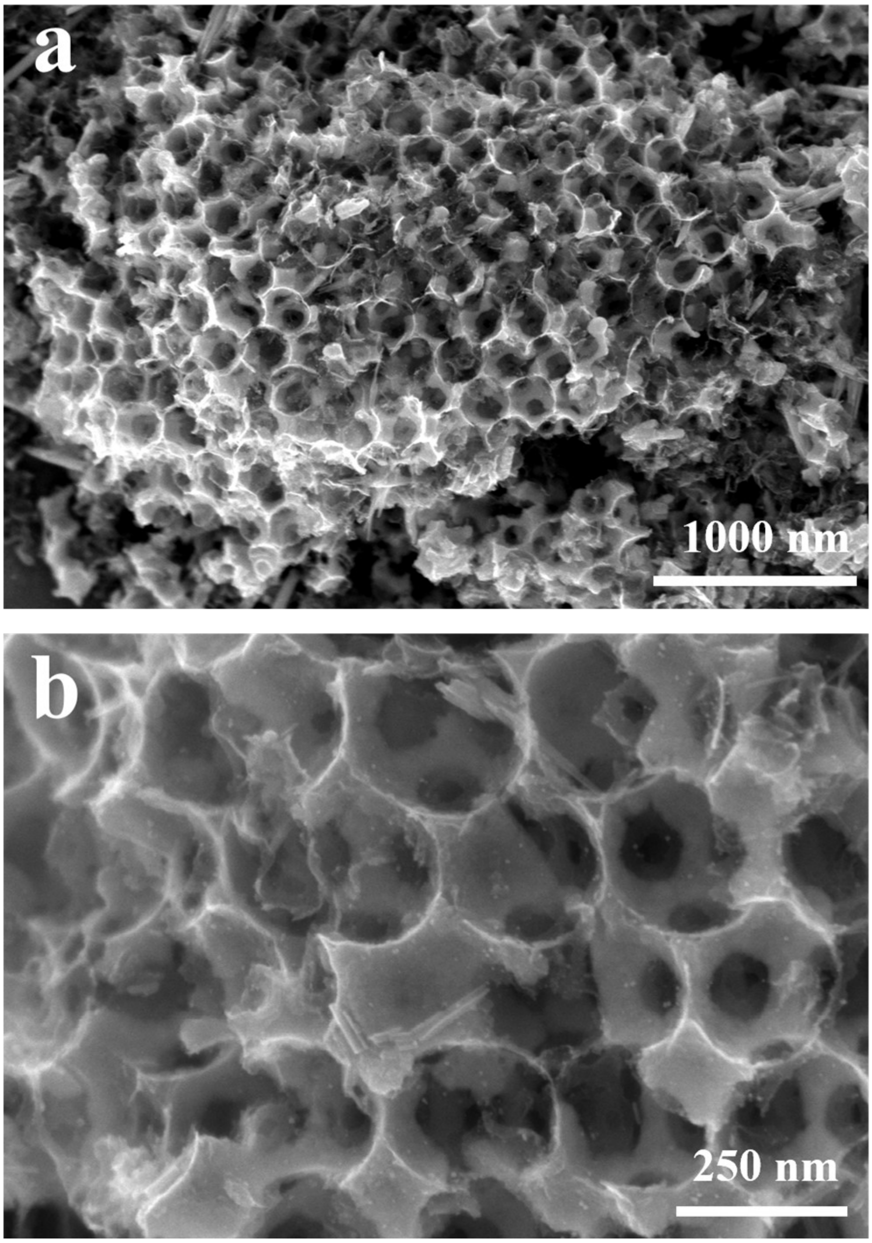

Figure S6. (a-d) SEM images of IrRu-$WO_{2.72}$-C at different magnifications.

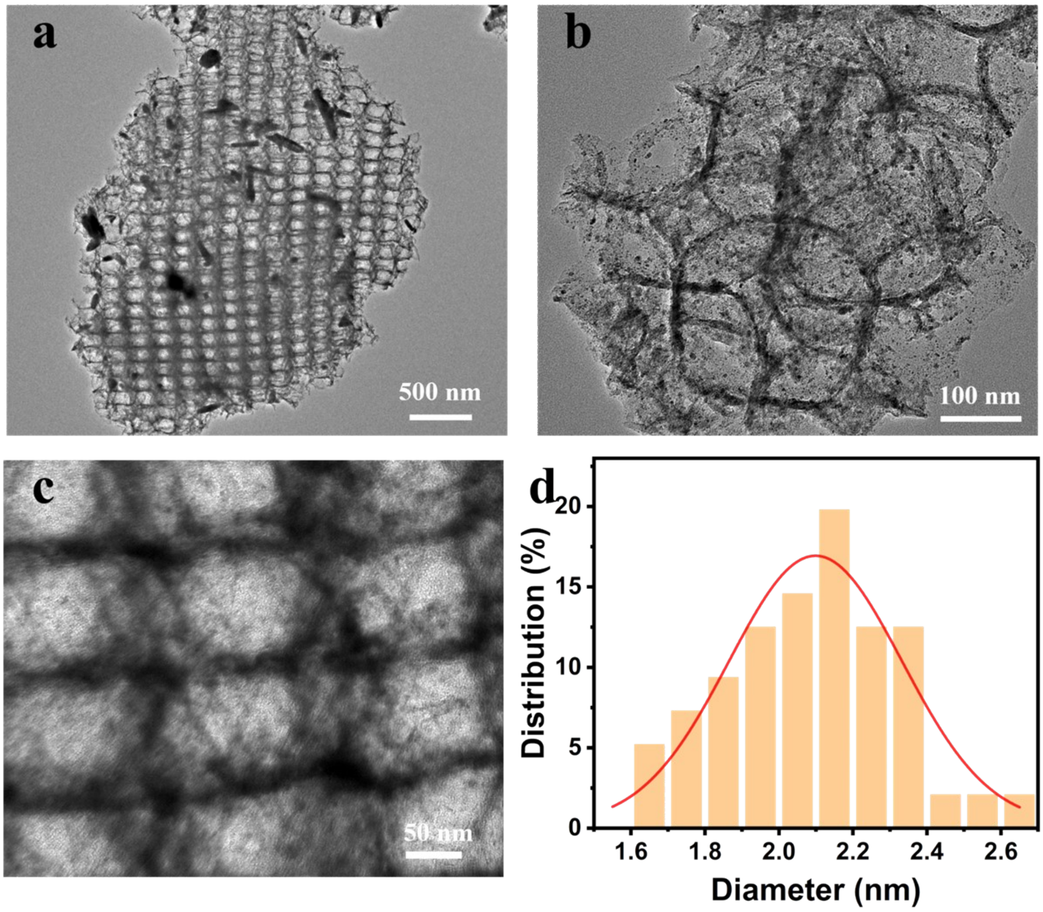

Figure S7. (a-c) TEM images of IrRu-$WO_{2.72}$-C at different magnifications. (d) The size distribution histograms of IrRu alloy clusters for IrRu-$WO_{2.72}$-C.

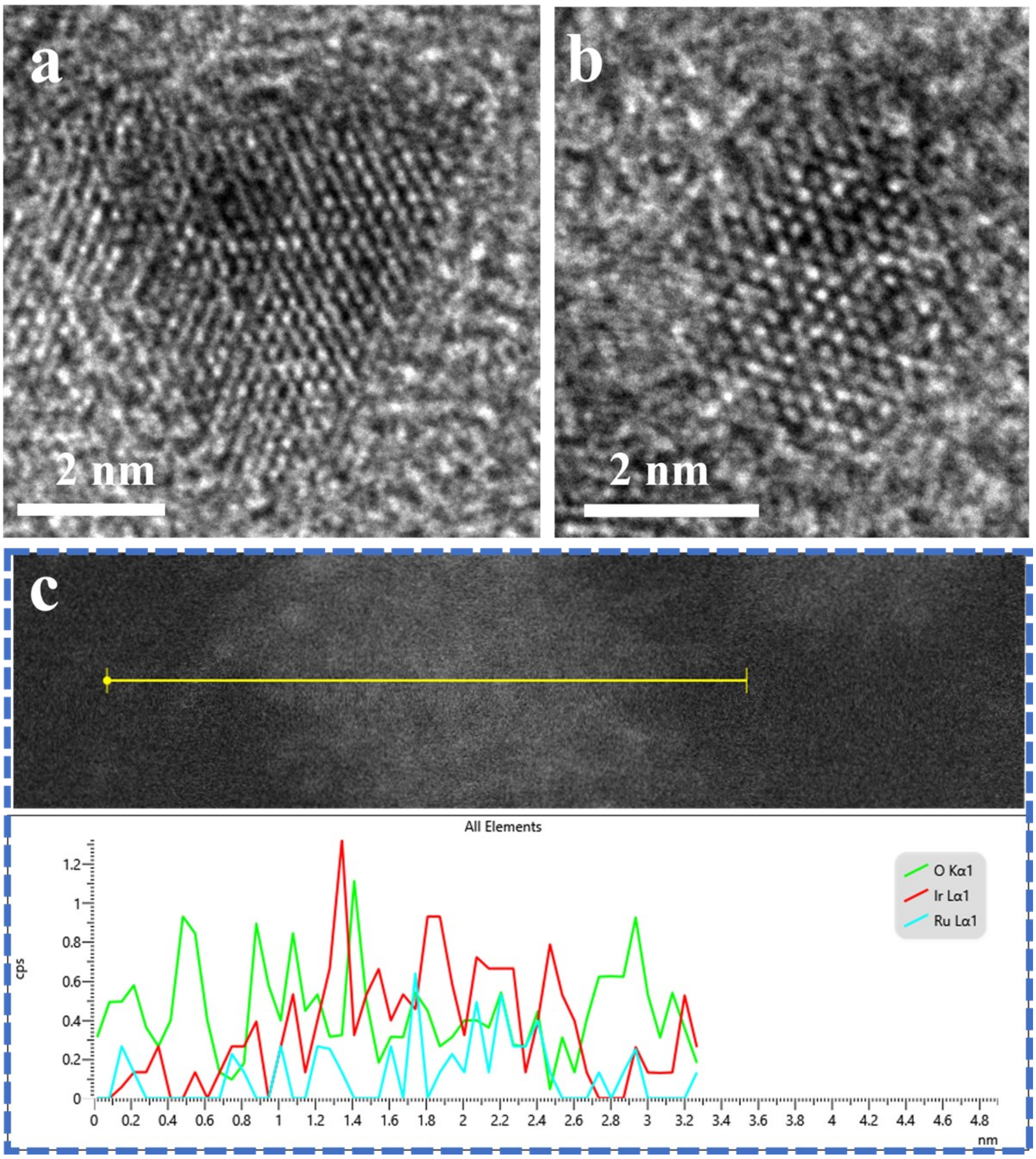

Figure S8. AC HAADF-STEM images (a, b) and liner elemental scanning profiles of IrRu clusters (c).

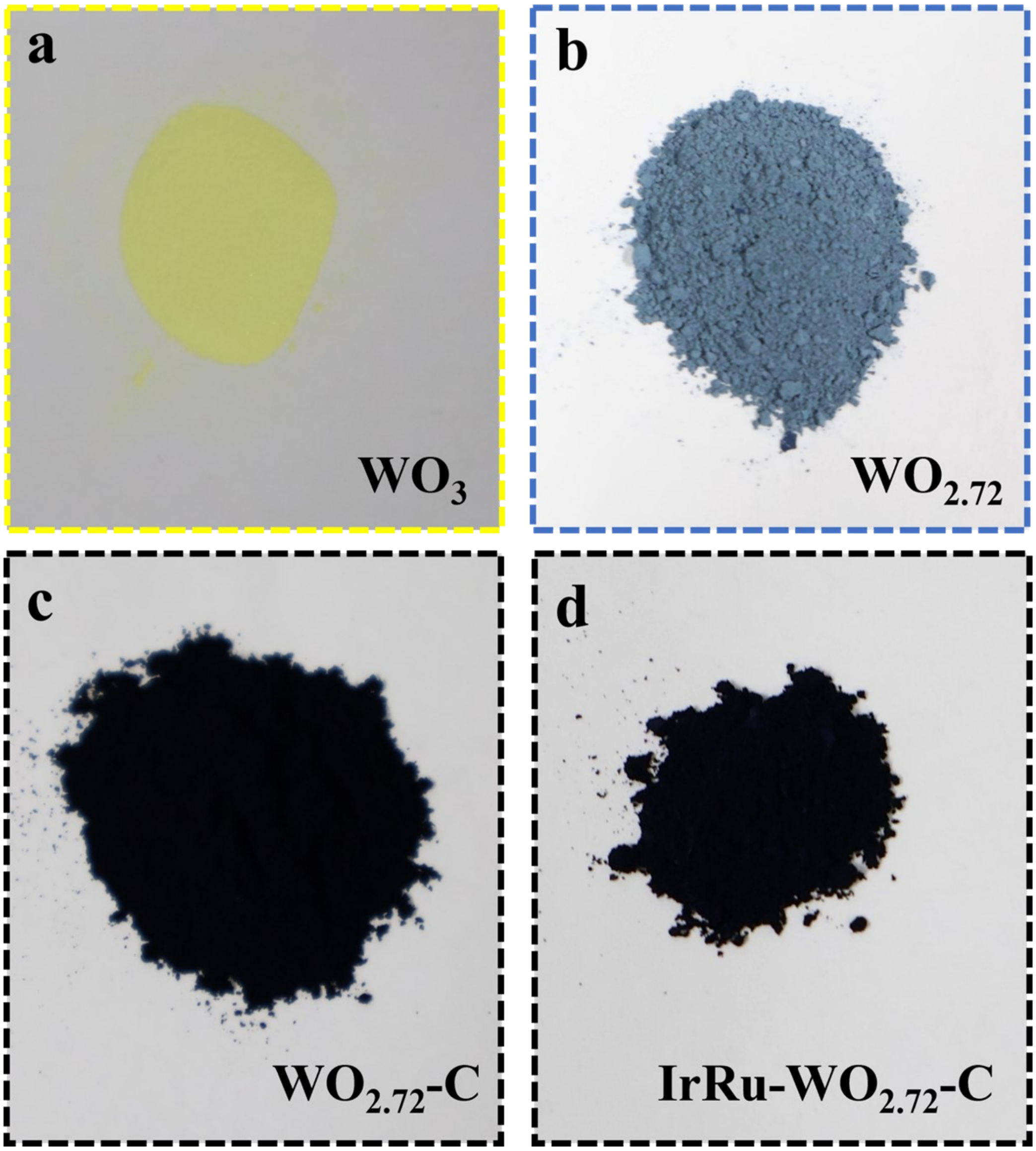

Figure S9. Digital photos of (a) WO_3, (b)$WO_{2.72}$, (c) $WO_{2.72}$-C and (d) IrRu-$WO_{2.72}$-C.

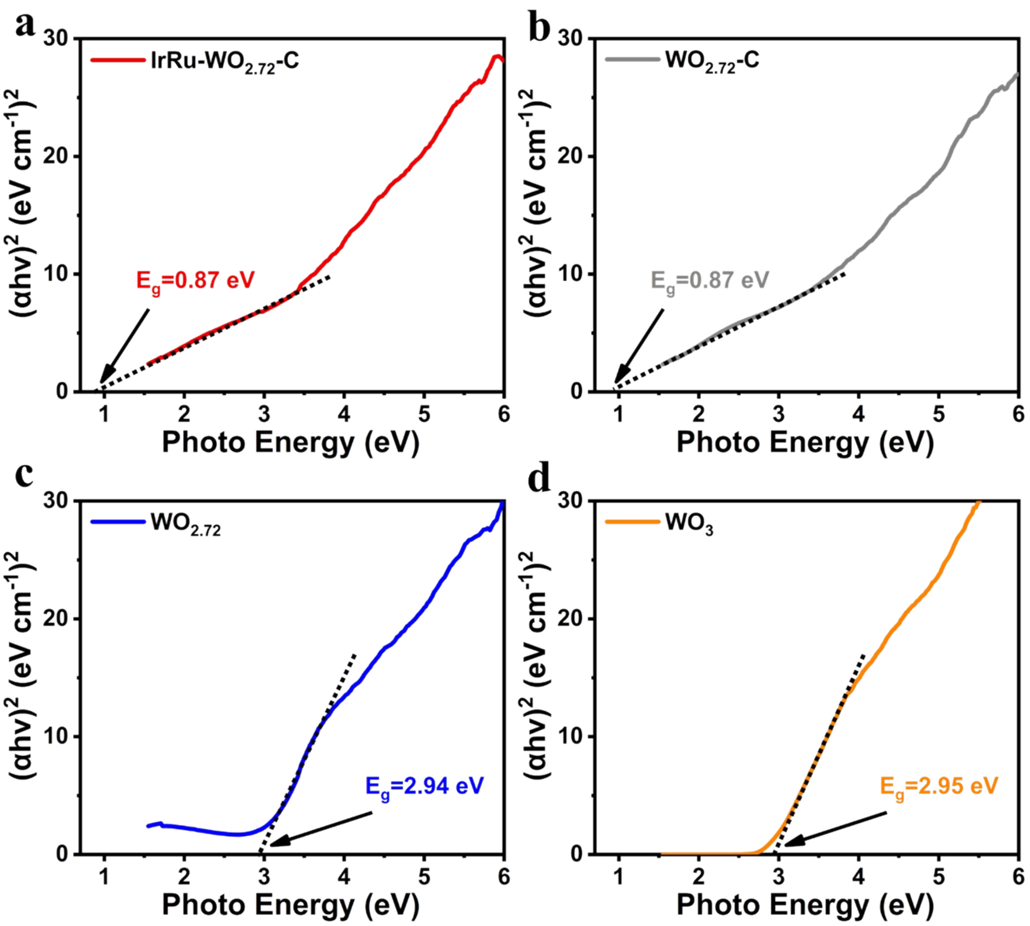

Figure S10. The Tauc plots of UV–vis spectra for (a) IrRu-$WO_{2.72}$-C, (b) $WO_{2.72}$-C, (c) $WO_{2.72}$ and (d) WO_3.

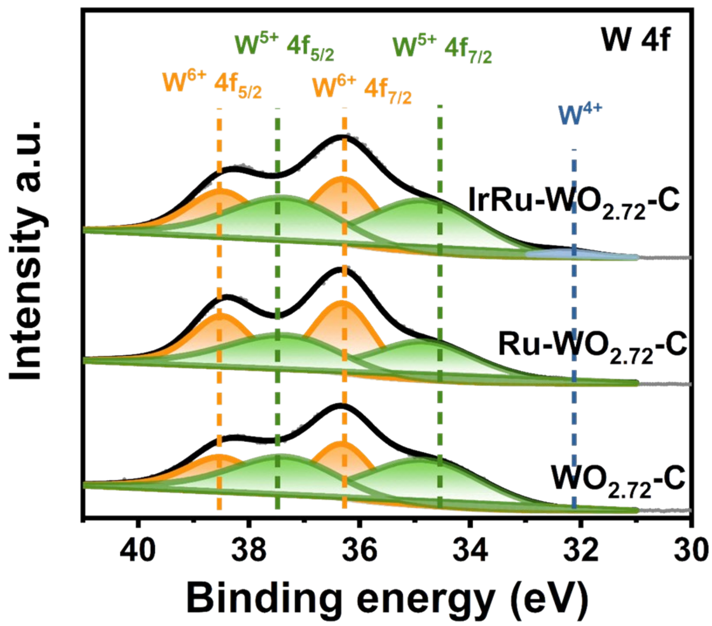

Figure S11. High-resolution XPS spectra of W 4f for IrRu-$WO_{2.72}$-C, Ru-$WO_{2.72}$-C and $WO_{2.72}$-C.

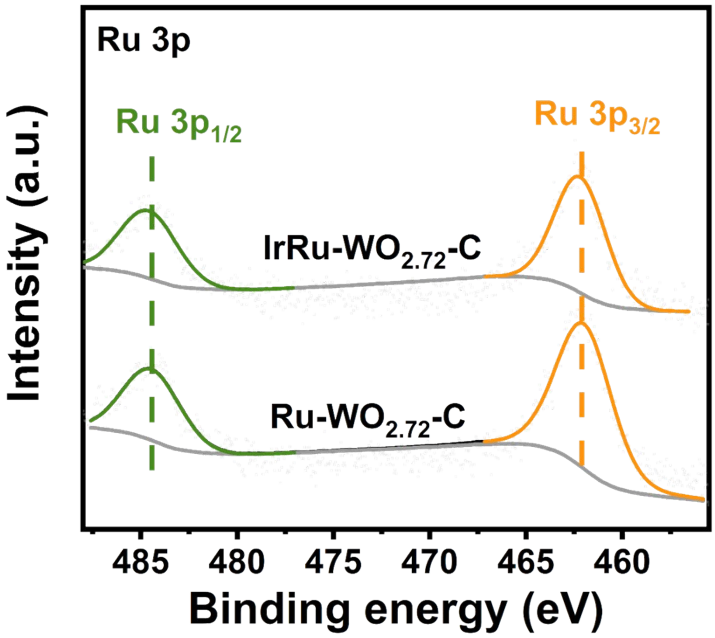

Figure S12. High-resolution XPS spectra of Ru 3p for IrRu-$WO_{2.72}$-C and Ru-$WO_{2.72}$-C.

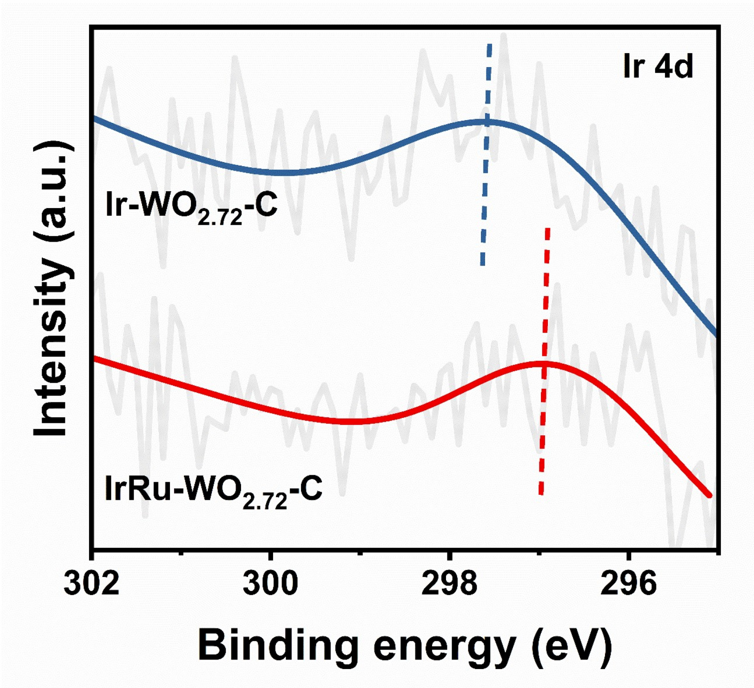

Figure S13. High-resolution XPS spectra of Ir 4d for IrRu-$WO_{2.72}$-C and Ir-$WO_{2.72}$-C.

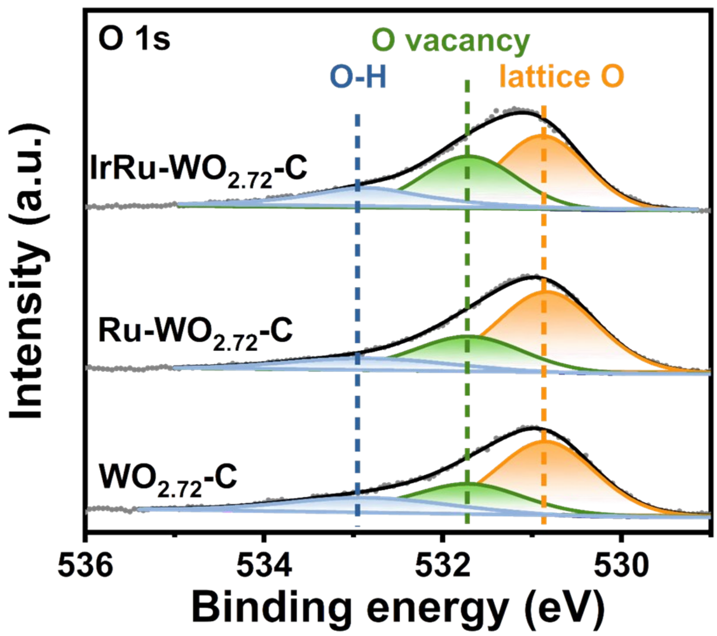

Figure S14. High-resolution XPS spectra of O 1s for IrRu-$WO_{2.72}$-C, Ru-$WO_{2.72}$-C and $WO_{2.72}$-C.

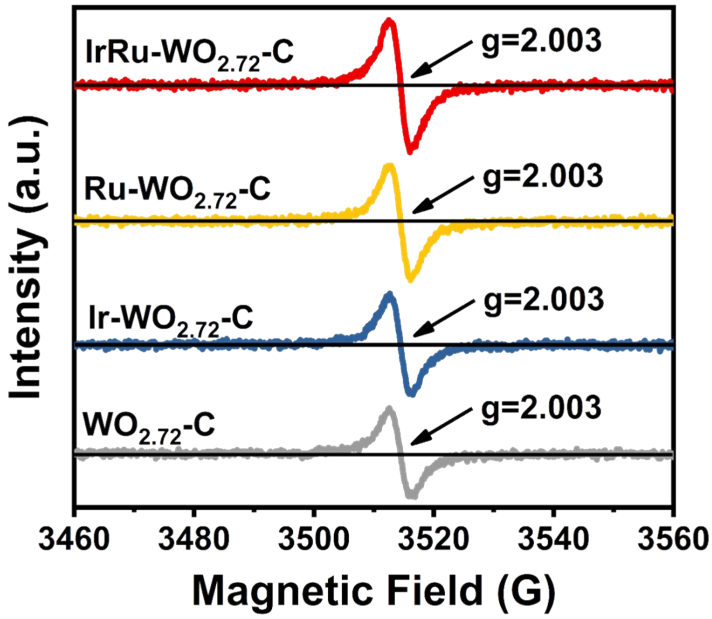

Figure S15. ESR spectra of IrRu-$WO_{2.72}$-C, Ir-$WO_{2.72}$-C, Ru-$WO_{2.72}$-C and $WO_{2.72}$-C.

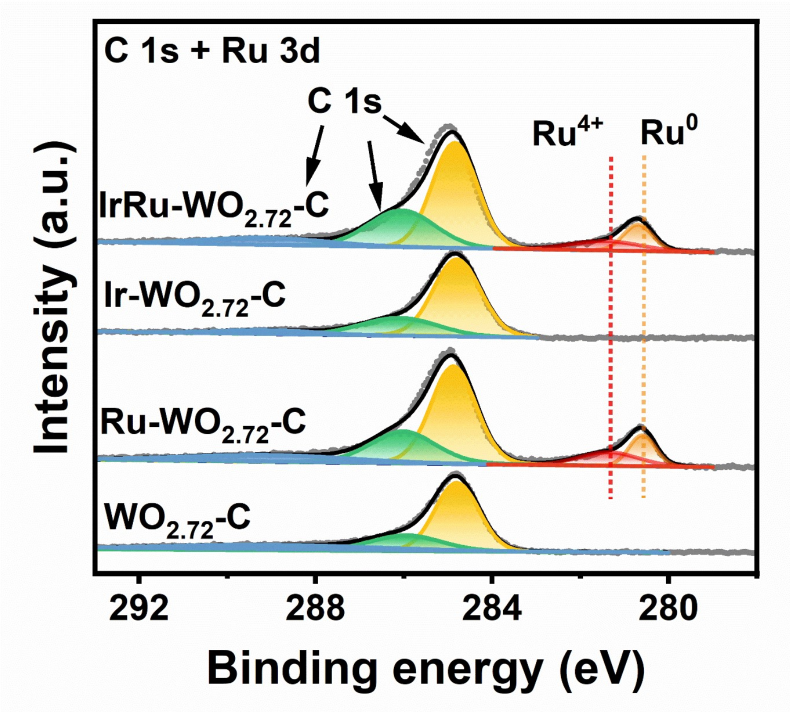

Figure S16. High-resolution XPS spectra of C 1s and Ru 3d for IrRu-$WO_{2.72}$-C, Ir-$WO_{2.72}$-C, Ru-$WO_{2.72}$-C and $WO_{2.72}$-C.

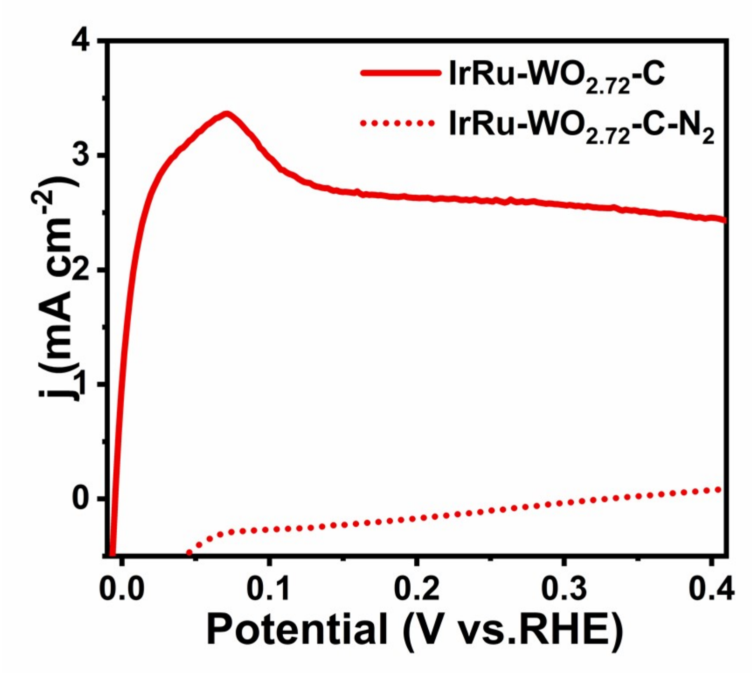

Figure S17. HOR polarization curves of IrRu-$WO_{2.72}$-C in N_2 or H_2 saturated 0.5 M H_2SO_4.

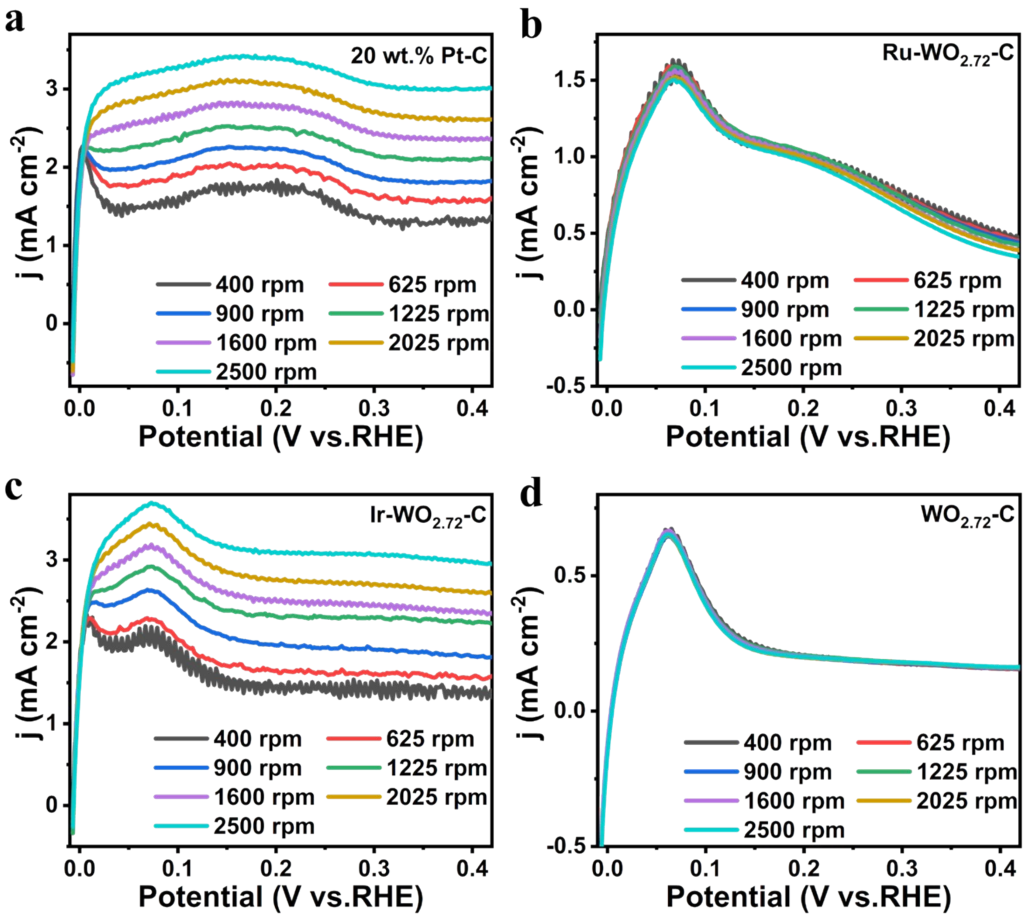

Figure S18. HOR polarization curves of (a) 20 wt.% Pt/C, (b) Ru-$WO_{2.72}$-C, (c) Ir-$WO_{2.72}$-C and (d) $WO_{2.72}$-C at different rotating speeds.

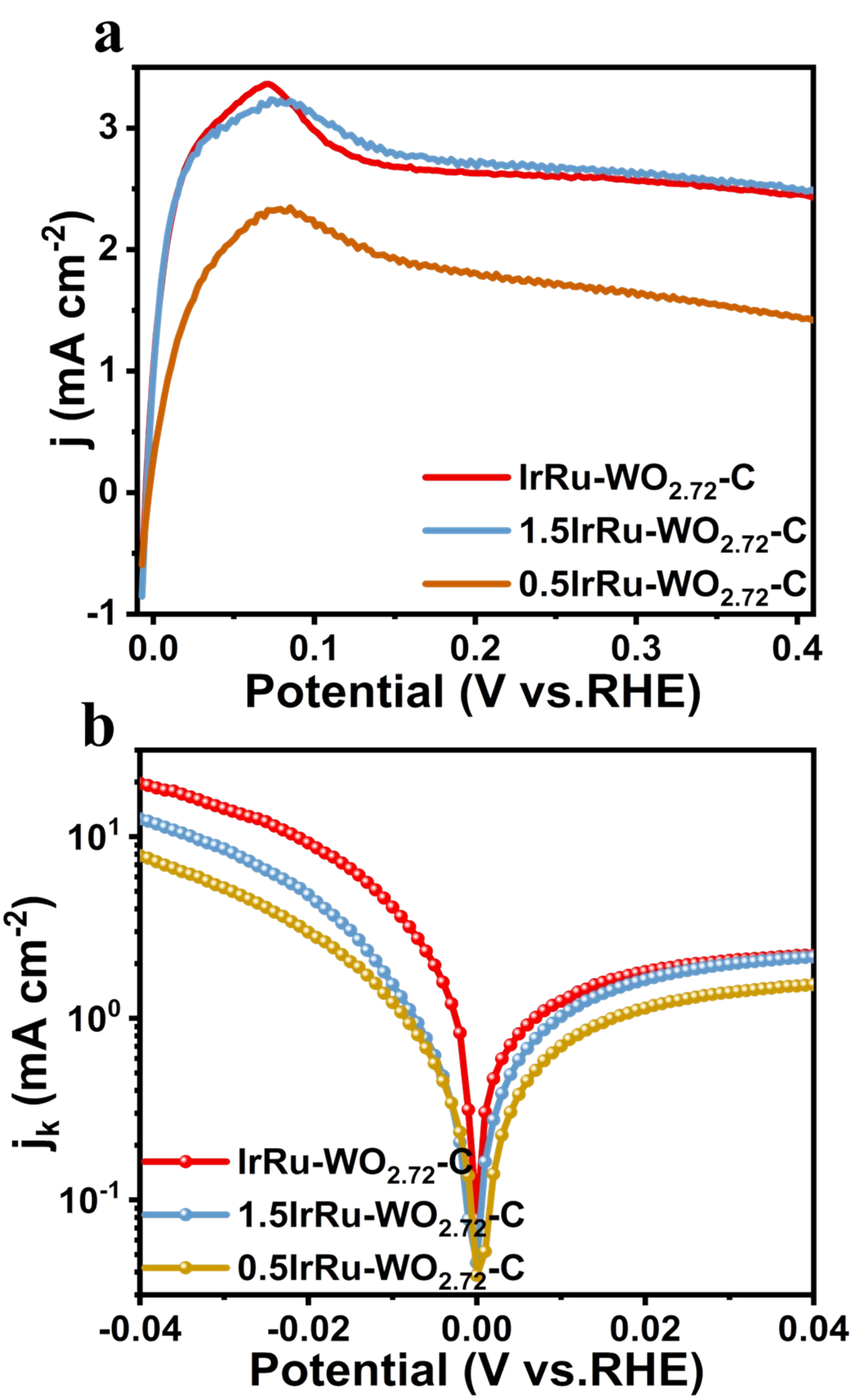

Figure S19. HOR polarization curves (a) and Tafel plots of kinetic current densities (b) for IrRu-$WO_{2.72}$-C, 0.5 IrRu-$WO_{2.72}$-C and 1.5 IrRu-$WO_{2.72}$-C.

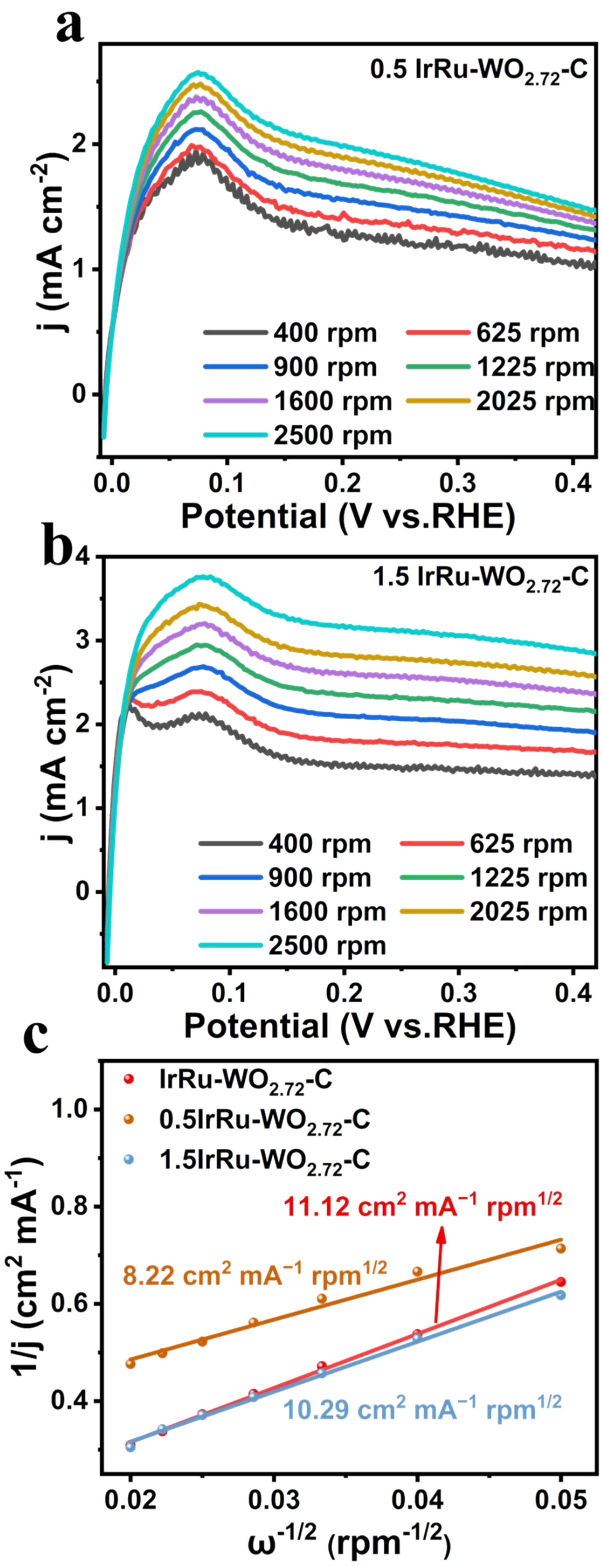

Figure S20. HOR polarization curves of (a) 0.5 IrRu-$WO_{2.72}$-C and (b) 1.5 IrRu-$WO_{2.72}$-C at different rotating speeds. (c) Koutecky−Levich plots of the catalysts at 0.15 V *vs* RHE.

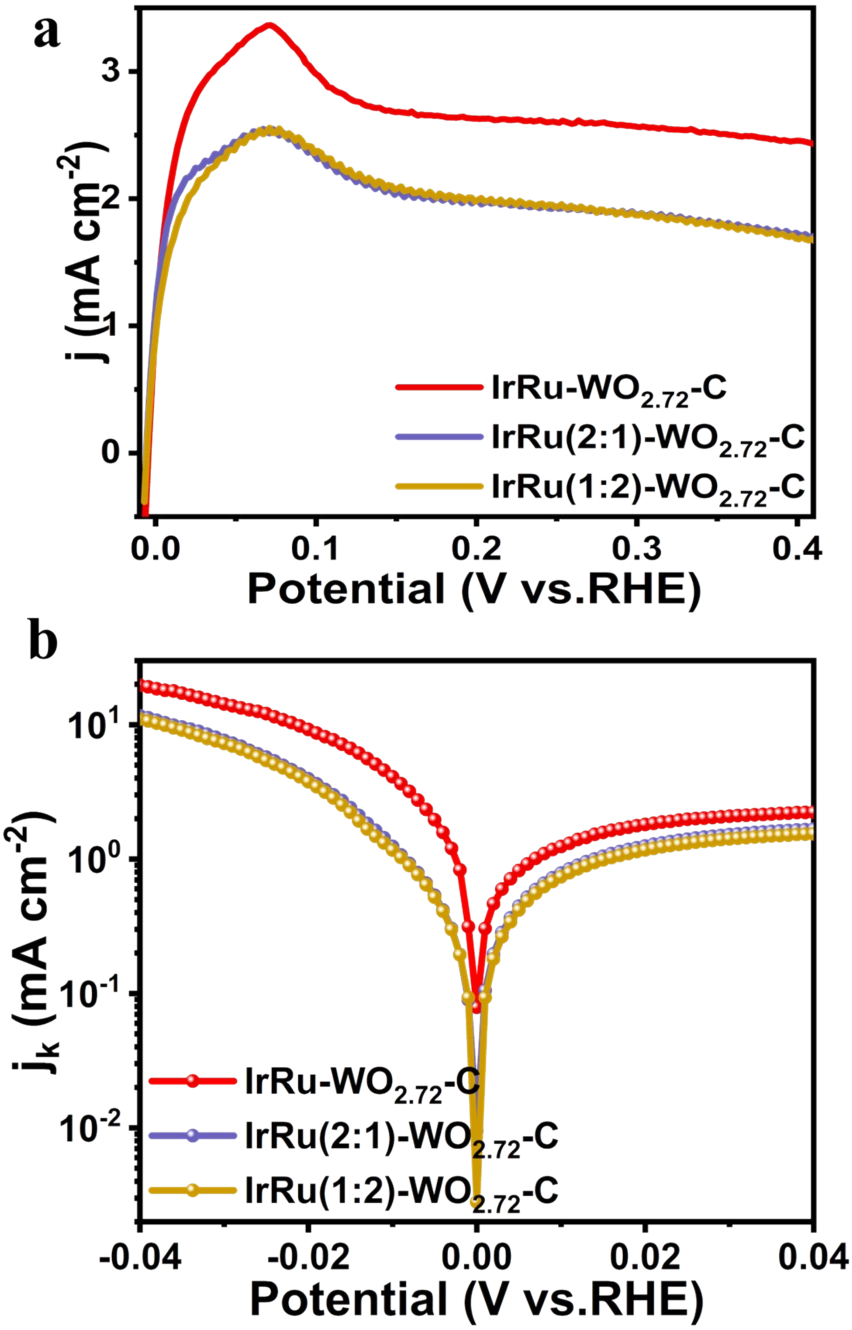

Figure S21. HOR polarization curves (a) and Tafel plots of kinetic current densities (b) for IrRu-$WO_{2.72}$-C, IrRu(2:1)-$WO_{2.72}$-C and IrRu(1:2)-$WO_{2.72}$-C.

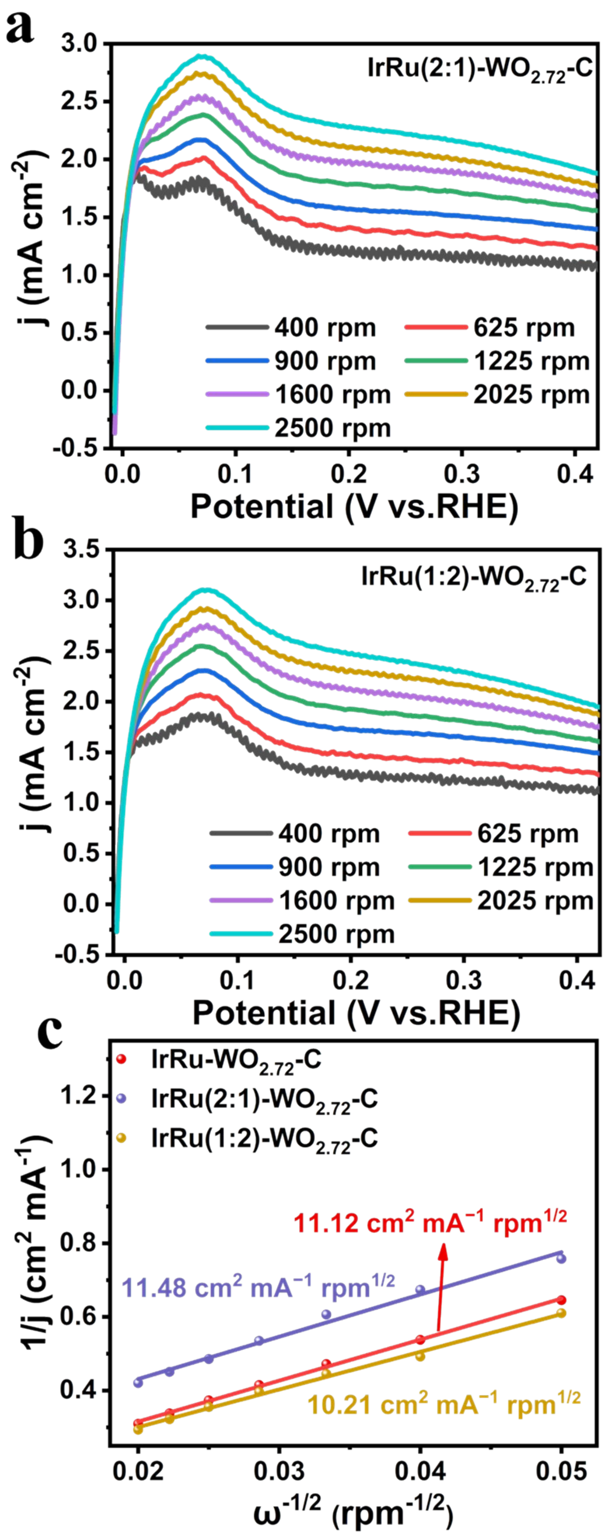

Figure S22. HOR polarization curves of (a) IrRu(2:1)-$WO_{2.72}$-C and (b) IrRu(1:2)-$WO_{2.72}$-C at different rotating speeds. (c) Koutecky-Levich plots of the catalysts at 0.15 V *vs.* RHE.

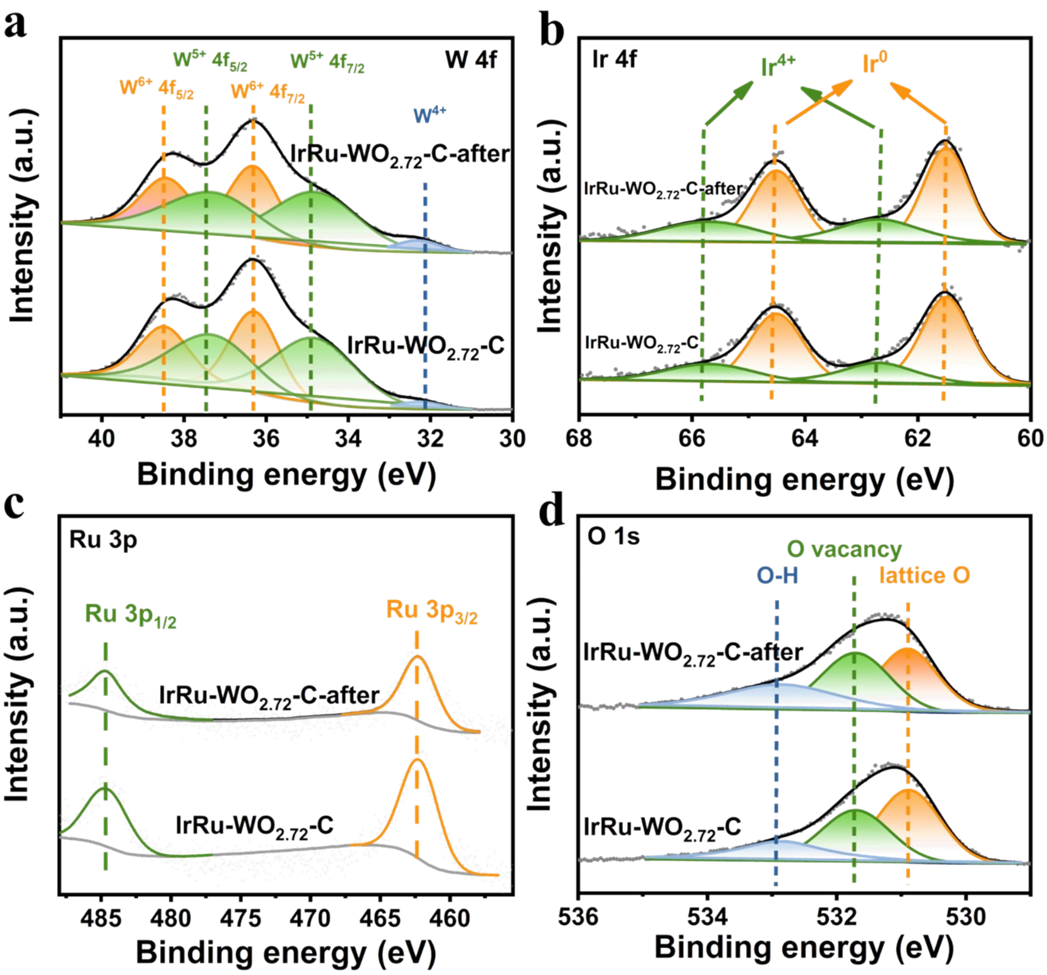

Figure S23. High-resolution XPS spectra of W 4f (a), Ir 4f (b), Ru 3p (c) and O1s (d) for IrRu-$WO_{2.72}$-C and after stability test named as IrRu-$WO_{2.72}$-C-after.

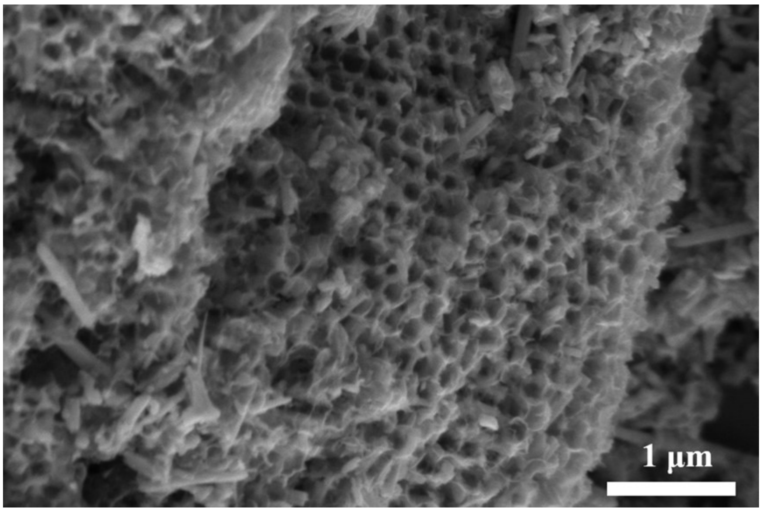

Figure S24. SEM image of IrRu-$WO_{2.72}$-C after stability test.

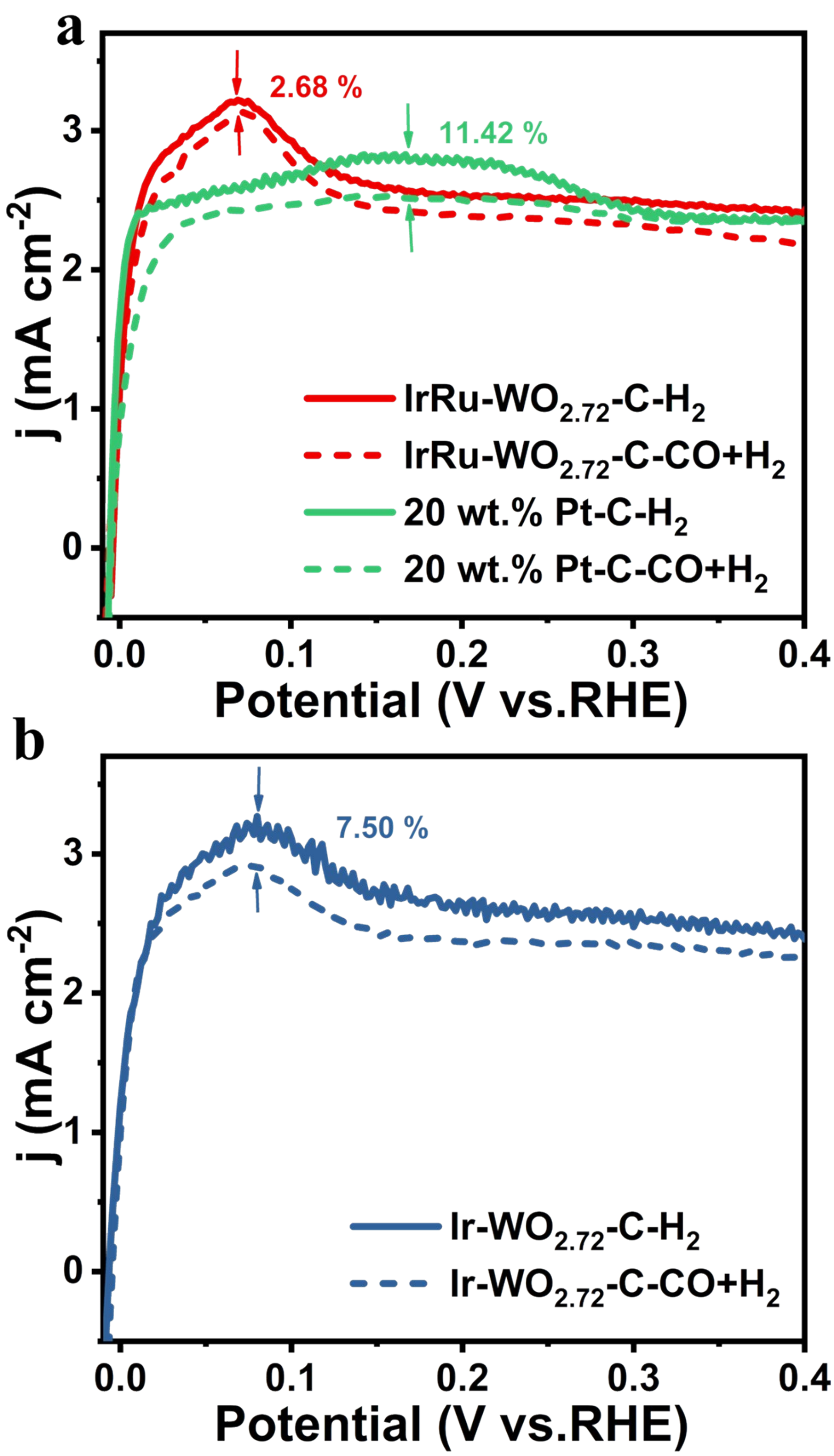

Figure S25. HOR polarization curves in H_2 and 1,000 ppm CO/H_2 saturated electrolytes for (a) 20 wt.% Pt/C, IrRu-$WO_{2.72}$-C and (b) Ir-$WO_{2.72}$-C.

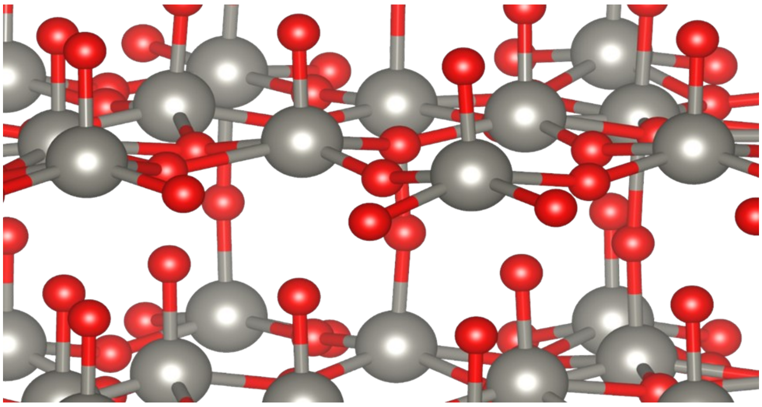

Figure S26. Side view of model structure for $WO_{2.72}$-C.

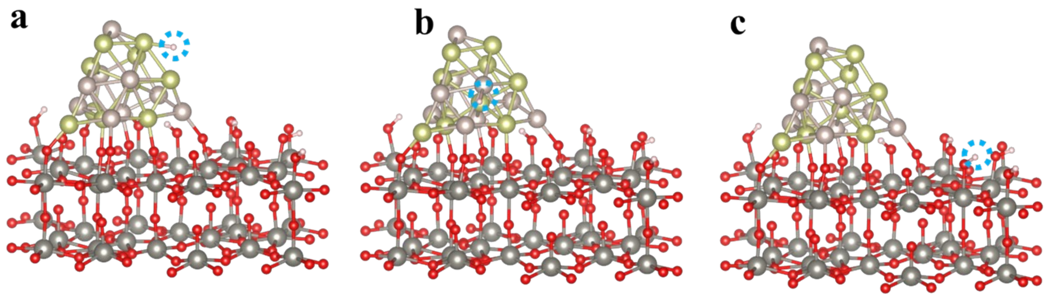

Figure S27. Side view of different H adsorption model structure on IrRu-$WO_{2.72}$-C.

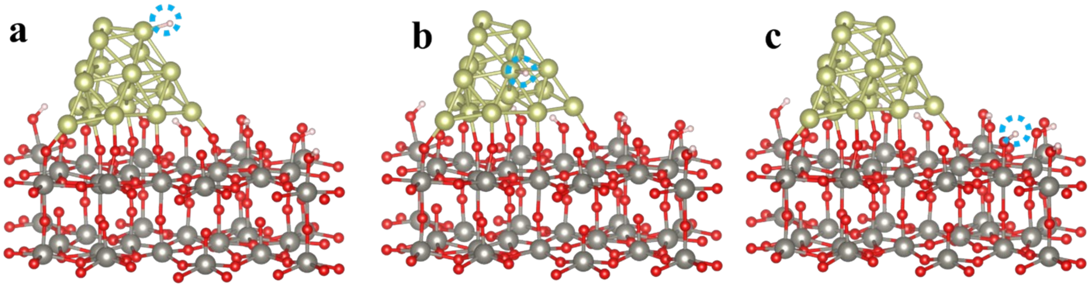

Figure S28. Side view of different H adsorption model structure on Ir-$WO_{2.72}$-C.

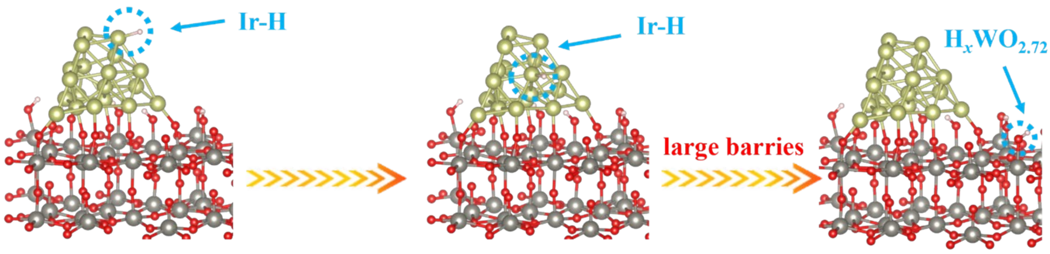

Figure S29. Schematic representation of the HOR mechanism and active hydrogen transfer pathway on the Ir-$WO_{2.72}$-C surface.

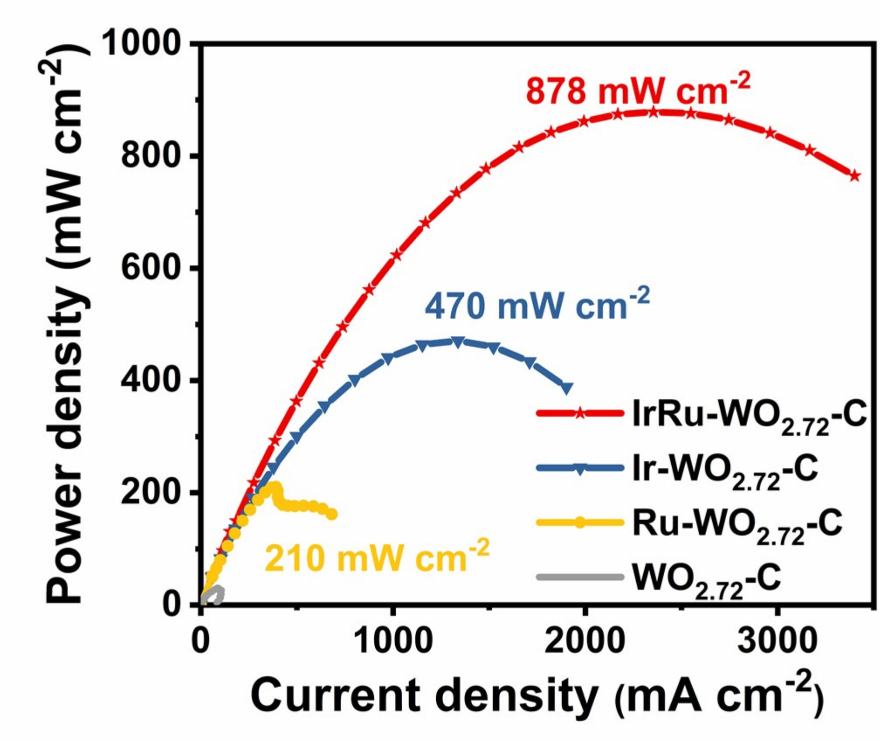

Figure S30. Power density curves of IrRu-$WO_{2.72}$-C, Ir-$WO_{2.72}$-C, Ru-$WO_{2.72}$-C and $WO_{2.72}$-C.

Table S1. The Ir and Ru loadings of samples tested by ICP-OES.

Samples	Percentage of Ir (wt.%)	Percentage of Ru (wt.%)
IrRu-$WO_{2.72}$-C	1.19	1.65
Ir-$WO_{2.72}$-C	1.65	/
Ru-$WO_{2.72}$-C	/	2.43

Table S2. The electrical conductivity values of as-prepared catalysts.

Samples	The electrical conductivity values (S cm^{-1})
WO_3	1.30×10^{-5}
IrRu-$WO_{2.72}$-C	9.29×10^{-5}
$WO_{2.72}$-C	0.22
IrRu-$WO_{2.72}$-C	2.41

Table S3. HOR performances in acidic media in the latest reported literature.

Catalyst	HOR current density（mA/cm^2）	The mass loading	Papers
$Ru@TiO_2$	~ 2.9	25.07μg$_{Ru}$ cm^{-2}	Nat. Catal. [1]
IrP_2-rGO	~ 2.5	8.84 μg$_{Ir}$ cm^{-2}	ACS Appl. Mater. Interfaces [2]
PdRu-WO_x/C	~ 3.1	49.44 μg$_{Pd}$ cm^{-2}	Catal. Today [3]
$Ni_xMo_{1-x}O_2$	~ 0.95	/	ACS Energy Lett. [4]
Rh-Rh_2O_3 NPs/C	~3.3	10.20 μg$_{Rh}$ cm^{-2}	J. Mater. Chem. A [5]
$Ir_{NP}@Ir_{SA}$-N-C	~2.7	5.61μg$_{Ir}$ cm^{-2}	Angew. Chem., Int. Ed. [6]
IrRu-N-C	~3.2	3.06 μg$_{Ir}$ cm^{-2}	Proc. Natl. Acad. Sci. U.S.A [7]
IrRu-$WO_{2.72}$-C	~3.35	5.41μg$_{Ir}$ cm^{-2}	This work

Table S4. The performance comparison and corresponding catalyst loading.

Catalyst	HOR current density (mA cm^{-2})	mass loading of catalyst (mg cm^{-2})	mass loading of precious metal ($\mu g_{Ir/Pt}$ cm^{-2})
IrRu-$WO_{2.72}$-C	~3.35	0.51	5.41
Ir-$WO_{2.72}$-C	~3.12	0.51	8.62
20 wt.% Pt-C	~2.68	0.51	102.04

References:

[1] Y.Y. Zhou, Z.Y. Xie, J.X. Jiang, J. Wang, X.Y. Song, Q. He, W. Ding, Z.D. Wei, Nat. Catal., 2020, **3**, 454-462.

[2] Z. Pu, T. Liu, W. Zhao, X. Shi, Y. Liu, G. Zhang, W. Hu, S. Sun, S. Liao, ACS Appl. Mater. Interfaces, 2020, **12**, 11737-11744.

[3] K. Kwon, S.A. Jin, K.H. Lee, D.J. You, C. Pak, Catal. Today, 2014, **232**, 175-178.

[4] H. Zeng, S. Chen, Y.Q. Jin, J. Li, J. Song, Z. Le, G. Liang, H. Zhang, F. Xie, J. Chen, Y. Jin, X. Chen, H. Meng, ACS Energy Lett., 2020, **5**, 1908-1915.

[5] M.K. Kundu, R. Mishra, T. Bhowmik, S. Barman, J. Mater. Chem. A, 2018, **6**, 23531-23541.

[6] X. Yang, Y. Wang, X. Wang, B. Mei, E. Luo, Y. Li, Q. Meng, Z. Jin, Z. Jiang, C. Liu, J. Ge, W. Xing, Angew. Chem. Int. Edit., 2021, **60**, 26177-26183.

[7] X. Wang, Y. Li, Y. Wang, H. Zhang, Z. Jin, X. Yang, Z. Shi, L. Liang, Z. Wu, Z. Jiang, W. Zhang, C. Liu, W. Xing, J. Ge, Proc Natl Acad Sci U S A, 2021, **118**, e2107332118.